European Heart Journal – Cardiovascular Imaging (2017) **18**, 538–548
doi:10.1093/ehjci/jew116

PET-measured longitudinal flow gradient correlates with invasive fractional flow reserve in CAD patients

Ines Valenta[1†], Alexander Antoniou[1†], Wael Marashdeh[1], Thorsten Leucker[2], Edward Kasper[2], Steven R. Jones[2], Robert F. Dannals[1], Lilja Solnes[1], Martin G. Pomper[1], and Thomas H. Schindler[1,2*]

[1]Division of Nuclear Medicine - Cardiovascular Section, Department of Radiology and Radiological Science, School of Medicine, Johns Hopkins University, JHOC 3225, 601 N. Caroline Street, Baltimore, MD 21287, USA; and [2]Division of Cardiology, Department of Medicine, Johns Hopkins University, Baltimore, MD, USA

Received 31 December 2015; accepted after revision 7 May 2016; online publish-ahead-of-print 18 June 2016

Aims We aimed to evaluate whether a PET-determined longitudinal decrease in myocardial blood flow (MBF) or gradient, assumed as a more specific flow parameter for epicardial resistance, correlates with invasively measured fractional flow reserve (FFR) in coronary artery disease (CAD) patients.

Methods and results In 29 patients with suspected or known CAD, myocardial perfusion and MBF in mL/g/min was determined with ^{13}N-ammonia PET/CT during regadenoson stimulation and at rest, and corresponding myocardial flow reserve (MFR = MBF stress/MBF rest) was calculated. MBF parameters were assessed in the myocardial region with stress-related perfusion defect and with stenosis ≥50% (Region 1), without defect but with stenosis ≥50% (Region 2), or without stenosis ≥50% (Region 3). Hyperaemic MBFs were significantly lower in the mid-distal than in the mid-left ventricular myocardium in Regions 1–3 [median and IQ range: 1.57 (1.24, 1.84) vs. 1.87 (1.61, 2.00), and 1.23 (1.11, 1.86) vs. 1.89 (1.80, 1.97), and 1.78 (1.48, 2.00) vs. 1.94 (1.84, 2.05) mL/g/min, $P < 0.0001$]. Resulting longitudinal MBF gradient during hyperaemic flows was more pronounced in Region 2 than in Regions 1 and 3, respectively [−0.46 (−0.70, −0.10) vs. −0.17 (−0.29, −0.11) and −0.15 (−0.25, −0.09) mL/g/min, respectively, $P < 0.01$]. There was a significant correlation between the hyperaemic longitudinal MBF gradient and FFR ($r = 0.95$; $P < 0.0001$), while this association was less pronounced for corresponding MFR ($r = 0.50$; $P = 0.006$).

Conclusion The observed close correlation between a longitudinal MBF gradient during hyperaemic flows and invasively measured FFR suggests the longitudinal flow gradient as an emerging non-invasive index of flow-limiting CAD.

Keywords CAD • circulation • coronary stenosis • flow gradient • microvascular function • myocardial blood flow • myocardial flow reserve • myocardial perfusion • PET

Introduction

Positron emission tomography (PET)-determined myocardial perfusion in conjunction with regional myocardial blood flow (MBF) quantification in mL/g/min emerges as a unique tool to evaluate the haemodynamic effects of each single epicardial narrowing in multivessel coronary artery disease (CAD).[1–5] The assessment of hyperaemic MBF and myocardial flow reserve (MFR) has also been appreciated to provide important prognostic information in patients with subclinical and clinically manifest CAD.[6–11] In the clinical setting, stress-induced regional myocardial perfusion defects commonly signify the 'culprit' or most advanced CAD lesion in multivessel disease, while reductions in hyperaemic MBFs are seen as non-specific as they may originate from both epicardial stenosis and/or microvascular dysfunction.[3,12,13] In this respect, Gould *et al.*[12] outlined that in the presence of an epicardial narrowing

* Corresponding author. Tel: +1 410 955 8449; Fax: +1 443 287 2933. E-mail: tschind3@jhmi.edu

† These authors contributed equally to this work.

exceeding 70% diameter stenosis, decreases in MFR <1.7 can be considered to reflect significant flow-limiting effects of the CAD lesion. Further help comes from PET flow measurements of an abnormal decrease in MBF from the base to the apex of the LV during hyperaemic flows, a so-called longitudinal MBF gradient.[1,14–18] This abnormal longitudinal MBF gradient during hyperaemic flow stimulation has been put forth to provide more specific information on flow-limiting effects of advanced CAD lesions than conventional interpretation of MFR alone.[1,14,15] In contrast to non-specific hyperaemic MBFs, invasively measured fractional flow reserve (FFR), ratio of the absolute distal coronary and aortic pressures measured during maximal hyperaemia, has been widely appreciated as an epicardial and lesion-specific flow index for CAD evaluation.[19]

To this end, we aimed to evaluate whether PET-determined longitudinal MBF gradient during hyperaemic flows correlates with invasively measured FFR in CAD patients.

Methods

Patient population

Twenty-nine patients (14 men, 15 women) with a median age of 68 (IQR: 55; 72) years and with stress-induced regional myocardial perfusion defects on ^{13}N-ammonia PET images were included for study purpose. Subsequently, invasive coronary angiography was performed within 20 days of the ^{13}N-ammonia PET study. Patients were considered for study purposes, if the culprit lesion, as evidenced by the stress-induced perfusion defect on ^{13}N-ammonia PET images, was accepted for percutaneous coronary intervention, followed by FFR measurement of a less severe lesion but ≥50% diameter stenosis in the proximal part of the left anterior descending (LAD) (Segments 12 and 13), or left circumflex (LCx) (Segments 18 and 19) according to the American College of Cardiology/American Heart Association guidelines.[20] Cardiovascular risk factors included the presence of arterial hypertension, smoking, type 2 diabetes mellitus, hypercholesterolaemia, obesity, or family history of CAD. Vasoactive medications such as calcium-channel blockers, angiotensin-converting enzyme inhibitors, statins, β-blockers, and diuretics were discontinued at least 24 h before the PET perfusion examination. All study participants refrained from caffeine-containing beverages for ≥24 h and from smoking for ≥12 h prior to the cardiac PET study. The study was approved by the Johns Hopkins Institutional Review Board (No. 00049877).

FFR measurements

Invasive quantitative coronary angiography was performed to assess the severity of epicardial lesions identified during invasive coronary angiography. Patients were considered for study purposes, if the non-culprit coronary artery lesions without stress-induced perfusion deficit but with ≥50% diameter stenosis was localized either in the proximal part of the LAD or in the LCx.[20] FFR was measured applying a 0.014-inch sensor-tipped guidewire, introduced through a 5- or 6-F guiding catheter. In order to stimulate hyperaemic flows, intracoronary bolus application of 150 μg adenosine in the left coronary artery was applied. FFR was determined as the ratio of mean distal intracoronary pressure, measured by pressure wire and mean arterial pressure measured with the coronary catheter. An FFR of ≤0.80 was considered a haemodynamically significant stenosis, and an FFR of >0.80 was non-significant.[21]

Myocardial perfusion PET study

^{13}N-ammonia PET determined myocardial perfusion and MBF in mL/min/g with serial image acquisition (64-slice Discovery Rx VCT PET/CT scanner, GE Healthcare), and a two-compartment tracer kinetic model, as described previously.[1,22] After acquiring the topogram applied to determine the axial field of view and a low-dose CT scan (120 kV, 30 mA) for attenuation correction, PET emission data were measured during shallow breathing. PET image acquisition during regadenoson-stimulated hyperaemia (0.4 mg intravenous bolus injection over 10 and 20 s interval) was started immediately following injection of ≈370 MBq ^{13}N-ammonia and also 45–60 min later at rest for a total duration of 18-min list-mode PET data acquisition, respectively. Myocardial perfusion images during vasomotor stress and at rest were evaluated visually on re-oriented short- and long-axis myocardial slices and semiquantitatively on the corresponding polar map from the last static 18-min transaxial PET image. Semiquantitative evaluation of ^{13}N-ammonia PET perfusion images was performed with a standard 20-segment model and a five-point grading system by two expert observers.[1,22] Summed stress score (SSS), summed rest score (SRS), and summed difference score (SDS) were determined. An SSS <4 was considered normal, 4–8 mildly abnormal, 9–13 moderately abnormal, and >13 severely abnormal perfusion defect. In addition, a SDS ≥2 signified a reversible perfusion defect, whereas <2 was deemed as normal. According to this, the extent of regional reversible perfusion defects on ^{13}N-ammonia PET images was scored according to the SDS value. An SDS of 2–4, >5–8, and >8 defined mild, moderate, and severe reversible perfusion defects, respectively.

MBF quantification

Left ventricular (LV) contours and input function region were obtained automatically with minimal operator intervention in QPET (Cedars-Sinai) as described previously.[23] Accordingly, cases were processed in batch mode and LV contours were positioned automatically. The LV contour was determined from the summed dynamic image data, skipping the first 2 min using the QPET algorithm.[23,24] The 3D region for the LV input function was automatically placed in the middle of the valve plane and was cylindric with a 1-cm radius and 2-cm length, with its long axis oriented along the long axis of the heart. The dynamic myocardial samples were obtained from the polar map by analysing all time frames within the fixed LV contour boundaries. QPET applies a two-compartment kinetic modelling for ^{13}N-ammonia as outlined by Choi *et al.*[25] Further, the uniform recovery coefficient of 0.76 to correct for partial-volume effects in the myocardium was applied assuming average myocardial thickness of 1 cm, respiratory motion of 5 mm, average cardiac motion of 7.5 mm, and intrinsic scanner spatial resolution of 4.8 mm.[23,26] Stress and rest MBF values in mL/g/min were calculated for each sample on the polar map. In order to minimize noise in the curves, the interpolation was used and computations were performed in 70 myocardial regions with equal surface areas. For each of these regions, regional flows were generated. Subsequently, these calculations were then interpolated using a surface-area-weighted bicubic method to determine flow values for each polar map sample.[23] Notably, the hyperaemic and rest MBF was computed within the whole LV region bounded by the LV plane. As regards the MFR, it was calculated by dividing each stress polar map sample by the rest samples at each point. Regional MBFs in mL/g/min of the myocardial regions subtended to the LAD, LCx, and RCA were averaged on a polar map, and the resulting mean MBF of the LV was defined as global MBF. In addition, two circumferential regions of interest were assigned to the mid- and the mid-distal portion of the LV myocardium on a 20-segment model (*Figure 1*). A decrease in MBF from mid- to mid-distal LV myocardium signified a decrease in longitudinal flow in mL/g/min that was defined as longitudinal MBF gradient in the LAD (anteroseptal, anterior), LCx (anterolateral, inferolateral or inferolateral, inferior depending on the vascular distribution of the LCx on invasive coronary angiography) and RCA (inferoseptal, inferior).[1,16] Alterations in the MBF gradient from

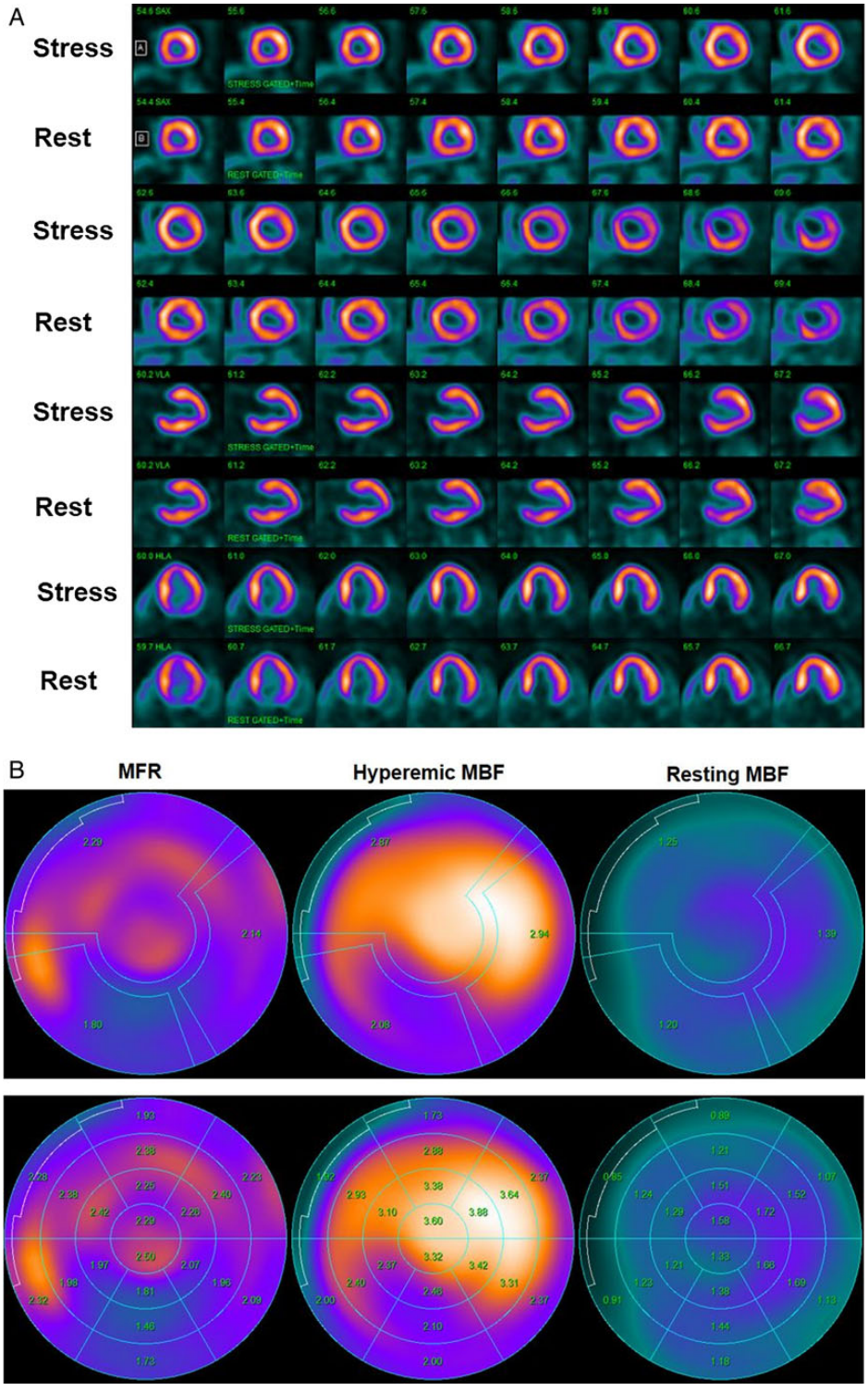

Figure 1 Normal myocardial perfusion and MBF study with ^{13}N-ammonia PET/CT in a 45-year-old women with atypical chest pain and borderline arterial hypertension. (*A*) Regadenoson-stress and rest ^{13}N-ammonia PET/CT images in corresponding short-axis (top), vertical long-axis (middle), and horizontal long-axis (bottom) slices. As can be appreciated, there is normal and homogeneous radiotracer uptake of the left ventricular wall on stress and rest ^{13}N-ammonia PET/CT, indicative of normal perfusion. (*B*) Regional MBF quantification signifies normal hyperaemic MBFs and MFR in all three major coronary artery territories of the LAD, LCx, and RCA with hyperaemic MBFs $\geq$1.8 mL/g/min (upper-middle panel). Calculated MFR is widely normal ($\geq$2.0) except for a borderline reduction in the RCA distribution (upper-right panel). Notably, there is no decrease but rather a mild increase in segmental MBF from the mid- to distal segments and, thus, no abnormal MBF gradient during hyperaemic MBFs is noted (lower-middle panel).

rest to hyperaemia were defined as Δlongitudinal MBF gradient (longitudinal MBF gradient during hyperaemia − longitudinal MBF gradient at rest).[17] Basal segments and the apical segment of the polar map, however, were not included for this analysis due to a possible count variability induced by the membranous septum, by a certain variability in locating the last apical slice, and by potential partial-volume errors resulting from object size at the apex as reported previously.[14] In order to avoid patient motion during PET acquisition, a torso and arm strap was applied. For every patient, sinograms of stress and rest image acquisition were reviewed for potential patient motion. In addition, the 36 dynamic frames were evaluated for appropriate LV contour alignment with the increasing radiotracer uptake. Studies with misalignment between LV contour and radiotracer uptake on any of the 36 dynamic frames, indicative of patient motion, were excluded for study purpose. At each MBF assessment, heart rate, blood pressure, and a 12-lead electrocardiogram were recorded continuously. From the average of heart rate and systolic blood pressure during the first 2 min of each image acquisition, the rate-pressure product (RPP) (heart rate × systolic blood pressure) was derived as an index of myocardial workload. To account for inter-individual variations in coronary driving pressure during hyperaemic flows, an index of coronary vascular resistance (CVR) was determined as the ratio of mean arterial blood pressure (mmHg) to MBF (mL/g/min).[1]

Statistical analysis

Since continuous variables are not always normally distributed, they are presented as median and interquartile range (IQR) (25th–75th percentile: Quartile 1, Quartile 3). For comparison of differences, we used the Mann–Whitney *U* test for independent samples (SPSS statistics 22.0, IBM, Armonk, NY, USA). A comparison of flow parameters among different myocardial territories was performed by Kruskal–Wallis one-way analysis of variance. Pearson correlation coefficients (*r*), assuming a linear regression and the standard error of the estimate (SEE), were calculated to investigate the associations between longitudinal MBF gradient and FFR, respectively. Using the Fisher's *r*-to-*z* transformation, the significance of differences between related correlations was determined. All test procedures were two-sided with a *P*-value of ≤ 0.05, indicating statistical significance.

Table 1 Characteristics of study population

	CAD patients
Numbers (*n*)	29
Age (years)	68 (55, 72)
Risk factors	
Hypertension (*n*)	10 (34%)
Smoking (*n*)	11 (38%)
Hypercholesterolaemia (*n*)	14 (48%)
Obesity (*n*)	9 (31%)
Family history of CAD (*n*)	8 (28%)
Diabetes mellitus (*n*)	7 (24%)

Values are median (Q1, Q3); numbers, *n* (%).

Results

Clinical characteristics

Table 1 denotes the clinical characteristics and cardiovascular risk factors of the study population. All patients had a history of effort-induced chest tightness: 19 with suspicion for CAD and 10 with known CAD. When a significant epicardial coronary artery lesion during coronary angiography was defined as ≥50% diameter stenosis, 17 patients had three-vessel disease, and 12 had two-vessel disease.

Stress-induced myocardial perfusion defects

In these patients with multivessel CAD, stress-rest ^{13}N-ammonia PET perfusion images identified regional reversible perfusion defects (abnormal SSS ≥4 and SDS ≥2) either in the LAD ($n = 20$) or in the LCx ($n = 9$) that defined the most advanced or culprit CAD lesion in multivessel disease as evidenced by coronary angiography. The mean SRS, SSS, and SDS were 1.5 ± 1.3, 6.4 ± 1.8, and 4.9 ± 1.6, respectively. There were 24% (7 of 29) mild, 62% (18 of 29) moderate, and 14% (4 of 29) severe reversible perfusion defects.

Haemodynamics and regional MBF

Table 2 demonstrates haemodynamics of the study population. During regadenoson-stimulated hyperaemia at the PET perfusion study, heart rate increased significantly compared with baseline, whereas there was a decrease in both systolic and diastolic blood pressures. Similarly, during adenosine-induced hyperaemic flow increases for the non-invasive FFR assessment, a significant increase in

Table 2 Haemodynamics in CAD patients during ^{13}N-ammonia PET/CT and invasive FFR measurement

	PET/CT	FFR	*P*-value
Rest-HR, bpm	74 (68, 77)	73 (67, 76)	0.332
Stress-HR, bpm	94 (90, 108)	95 (90, 105)	0.628
Rest-SBP, mmHg	136 (123, 140)	137 (125, 144)	0.956
Stress-SBP, mmHg	118 (115, 134)	119 (116, 133)	0.740
Rest-DBP, mmHg	69 (64, 89)	70 (64, 88)	0.883
Stress-DBP, mmHg	65 (62, 72)	66 (63, 73)	0.858
Rest-RPP	9720 (9282, 10 138)	9590 (8925, 10 336)	0.911
Stress-RPP	12 192 (10 591, 13 608)	12 250 (10 556, 12 971)	0.749

Values are median (Q1, Q3); *P*-values vs. controls (Mann–Whitney *U* test for independent samples).
HR, heart rate; SBP, systolic blood pressure; DBP, diastolic blood pressure; RPP, rate-pressure product (HR × SBP).

Table 3 **Myocardial flow parameters in territories with and without stress-induced perfusion defects (PD) during PET/CT**

	Region with PD (R1)	Region without PD and stenosis ≥50% (R2)	*P*-values (R2 vs. R1)	Region without both PD and stenosis ≥50% (R3)	*P*-values (R3 vs. R1)	*P*-values (R3 vs. R2)
Regional flow						
MBF rest	0.71 (0.67, 0.80)	0.76 (0.65, 0.90)	0.202	0.75 (0.68, 0.81)	0.264	0.844
MBF stress	1.44 (1.23, 1.72)	1.53 (1.38, 2.04)	0.119	1.60 (1.37, 1.82)	0.202	0.782
MFR	1.97 (1.71, 2.36)	2.02 (1.92, 2.41)	0.360	2.23 (1.76, 2.37)	0.505	0.757
Longitudinal flow						
MBF at rest						
Mid-LV segment	0.90 (0.76, 0.99)	0.92 (0.77, 1.02)	0.594	0.90 (0.82, 0.99)	0.416	0.762
Mid-distal segment	0.89 (0.78, 0.97)	0.86 (0.72, 0.97)	0.877	0.88 (0.78, 1.00)	0.436	0.537
Gradient	−0.01 (−0.05, 0.02)	−0.03 (−0.04, 0.02)	0.412	−0.03 (−0.06, −0.00)	0.966	0.424
MBF during stress						
Mid-LV segment	1.87 (1.61, 2.00)	1.89 (1.80, 1.97)	0.283	1.94 (1.84, 2.05)	0.322	0.913
Mid-distal segment	1.57 (1.24, 1.84)	1.23 (1.11, 1.86)	0.755	1.78 (1.48, 2.00)	0.192	0.142
Gradient	−0.17 (−0.29, −0.11)	−0.46 (−0.70, −0.10)	*0.013*	−0.15 (−0.25, −0.09)	0.333	*0.002*
ΔGradient	−0.19 (−0.26, −0.11)	−0.41 (−0.67, −0.12)	*0.018*	−0.13 (−0.22, −0.07)	0.285	*0.002*
CVR at rest						
Mid-LV segment	114 (89, 135)	98 (84, 129)	0.610	97 (86, 126)	0.496	0.849
Mid-distal segment	113 (90, 133)	113 (90, 132)	0.873	105 (85, 133)	0.615	0.714
Gradient	0.63 (−2.79, 6.15)	4.86 (1.24, 8.57)	0.200	3.93 (0.00, 7.92)	0.490	0.482
CVR during stress						
Mid-LV segment	44 (43, 53)	45 (40, 49)	0.219	43 (41, 45)	0.206	0.945
Mid-distal segment	53 (47, 65)	66 (45, 75)	0.237	47 (44, 59)	0.150	*0.014*
Gradient	3.93 (3.13, 10.83)	20.56 (1.48, 28.11)	*0.011*	3.96 (2.23, 6.83)	0.390	*0.001*
ΔCVR gradient	5.00 (2.20, 7.60)	9.49 (1.21, 20.58)	*0.051*	2.00 (−3.96, 4.37)	0.149	*0.003*

Values are median (Q1, Q3).
Region 1 (R1), stress-induced perfusion defect (PD); Region 2 (R2), no stress-induced perfusion defect and stenosis ≥50%; Region 3 (R3), no stress-induced perfusion defect without stenosis ≥50%; MBF, myocardial blood flow (mL/g/min); MFR, myocardial flow reserve; CVR, coronary vascular resistance (mmHg/mL/g/min).
P-values according to Mann–Whitney *U* test for independent samples.

heart was also appreciated, while systolic and diastolic blood pressures decreased. The RPP at rest and during pharmacologic vasodilation was similar between both conditions of hyperaemic flow stimulation, indicating comparable haemodynamic study conditions. As regards PET-determined regional MBFs at rest, they did not differ among Regions 1–3 (*Table 3*). Compared with Region 3, hyperaemic MBFs and MFR progressively but non-significantly declined in Regions 2 and 1, respectively (*Table 3*). In addition, the regional CVR (mean arterial blood pressure/MBF) widely mirrored the MBF values during hyperaemic flow stimulation and at rest for each region studied.

Longitudinal MBF gradient

Resting MBF was non-significantly lower in the mid-distal than in the mid-LV myocardium in Regions 1–3 [median 0.89 (IQR: 0.78, 0.97) mL/g/min vs. 0.90 (IQR: 0.76, 0.99) mL/g/min, 0.86 (0.72, 0.97) vs. 0.92 (0.77, 1.02) mL/g/min, and 0.88 (0.78, 1.00) vs. 0.90 (0.82, 0.99) mL/g/min, respectively]. This manifested in small and similar resting longitudinal MBF gradients between the three regions (*Table 3*). During regadenoson-stimulated hyperaemic flows, the decrease in longitudinal flow from the base to apex direction was more pronounced in Region 2 than in Regions 1 and 3, respectively, while it did not differ significantly between Regions 1 and 3 [1.89 (1.80, 1.97) to 1.23 (1.11, 1.86) mL/g/min vs. 1.87 (1.61, 2.00) to 1.57 (1.24, 1.84) mL/g/min and 1.94 (1.84, 2.05) to 1.78 (1.48, 2.00) mL/g/min, respectively]. This resulted in a significantly higher hyperaemic longitudinal MBF gradient and Δlongitudinal MBF gradient in Region 2 when compared with Regions 1 and 3, respectively (*Table 3*; *Figures 2* and *3*). Although the hyperaemic longitudinal MBF gradient and Δlongitudinal MBF gradient were higher in Region 1 than in Region 3, respectively, they did not reach statistical significance.

Correlations between regional MFR, longitudinal MBF gradient, and FFR

In order to evaluate a possible correlation between hyperaemic flow parameters and flow-limiting effects of epicardial stenosis, the invasively measured FFR in Region 2 was related to the corresponding hyperaemic MBF gradient and Δlongitudinal MBF and MFR, respectively. As it can be appreciated in *Figure 4A* and *B*, the severity of FFR was closely paralleled by the extent of hyperaemic longitudinal MBF and Δlongitudinal MBF, respectively ($r = 0.95$ and 0.94; both $P < 0.0001$). Conversely, FFR also correlated with decreases in hyperaemic MBFs and MFR, respectively ($r = 0.63$, $P < 0.0001$ and $r = 0.50$, $P = 0.006$), while these associations were less pronounced as observed for the longitudinal MBF gradient (*Figure 4C* and *D*). The correlation coefficients between the FFR and hyperaemic longitudinal MBF proved to be significantly higher than between FFR and hyperaemic MBF and MFR, respectively ($z = 3.93$ and 4.62; both $P < 0.0001$). In addition, we aimed to evaluate whether the hyperaemic longitudinal MBF gradient was dependent also of the increase in hyperaemic flows during regadenoson stimulation. The extent of the longitudinal MBF gradient during hyperaemic flows, however, did not correlate significantly with the increases in hyperaemic MBFs in the mid-LV of the corresponding region ($r = 0.33$, $P = 0.084$), suggesting a predominant uncoupling of the hyperaemic longitudinal MBF gradient from the flow increase.

Discussion

The observations of the current investigations are unique in that they demonstrate a significant association between invasively measured FFR, as a specific functional parameter of the epicardial resistance in CAD, and a post-stenotic longitudinal MBF from the mid- to mid-distal LV myocardium. Such observations suggest indeed that the observed hyperaemic longitudinal MBF gradient is predominantly caused by abnormal increases in epicardial resistance to coronary flow due to focal CAD lesions. These results accord with previous investigations relating the longitudinal flow gradient during hyperaemic flow to abnormalities in epicardial vasomotor function and to diffuse and/or focal CAD[1,14,16,18,22] but expand these observations to an association between alterations in invasive FFR and hyperaemic longitudinal MBF gradient. Thus, while stress-induced regional perfusion defects signify the most advanced CAD lesion in multivessel disease, an abnormal hyperaemic MBF gradient may serve as a useful tool for the specific detection of flow-limiting CAD lesions of less severity and without regional perfusion defect that warrants further clinical investigations.

As regards PET-determined regional hyperaemic MBFs and MFR, respectively, they progressively but non-significantly increased from the region with stress-related perfusion defect to the remote region without perfusion defect but with or without stenosis ≥50%, respectively. Someone might have expected more pronounced and statistically significant differences in mean hyperaemic MBFs and MFR among these regions that is likely related to relatively small sample size of the study population and an observed wide range of individual hyperaemic MBF values.[2,27] Increases in severity of FFR, however, were paralleled by a progressive increase in the magnitude of a post-stenotic longitudinal MBF gradient in the presence of epicardial stenosis of predominantly intermediate severity. Such observations in fact may agree with the Hagen–Poiseuille law.[14,15,19,28] According to the latter, the resistance to flow depends on the length of the tube, the flow velocity and, importantly, inversely on the fourth power of the vessel diameter. And indeed, in the current study, the extent of the hyperaemic longitudinal MBF gradient was related to the severity of the FFR, reflecting the downstream effects of epicardial stenosis on flow, and thus the severity of CAD focal epicardial narrowing. As regards the flow velocity, however, the extent of the longitudinal MBF gradient during hyperaemic flows did not significantly correlate with the increases in hyperaemic MBFs in the mid-LV of the corresponding region. This contrast recent observations in the assessment of the longitudinal flow gradient in individuals with subclinical CAD.[22] According to the Hagen–Poiseuille law, the coronary driving pressure increases in proportion of the flow velocity. However, beyond a critical velocity, this relationship will no longer hold true for a given stenosis and the laminar flow will turn into tubular flow with a pressure drop and decrease in flow.[15,29,30] Consequently, in the current investigation, advanced epicardial narrowing is likely to have suspended, at least in part, the dependency of the longitudinal MBF gradient from the velocity of the hyperaemic flow increase in these patients with multivessel disease as opposed to non-obstructive CAD.[22]

Interestingly, in regions with stress-induced regional perfusion defects on ^{13}N-ammonia PET images, the abnormal longitudinal MBF

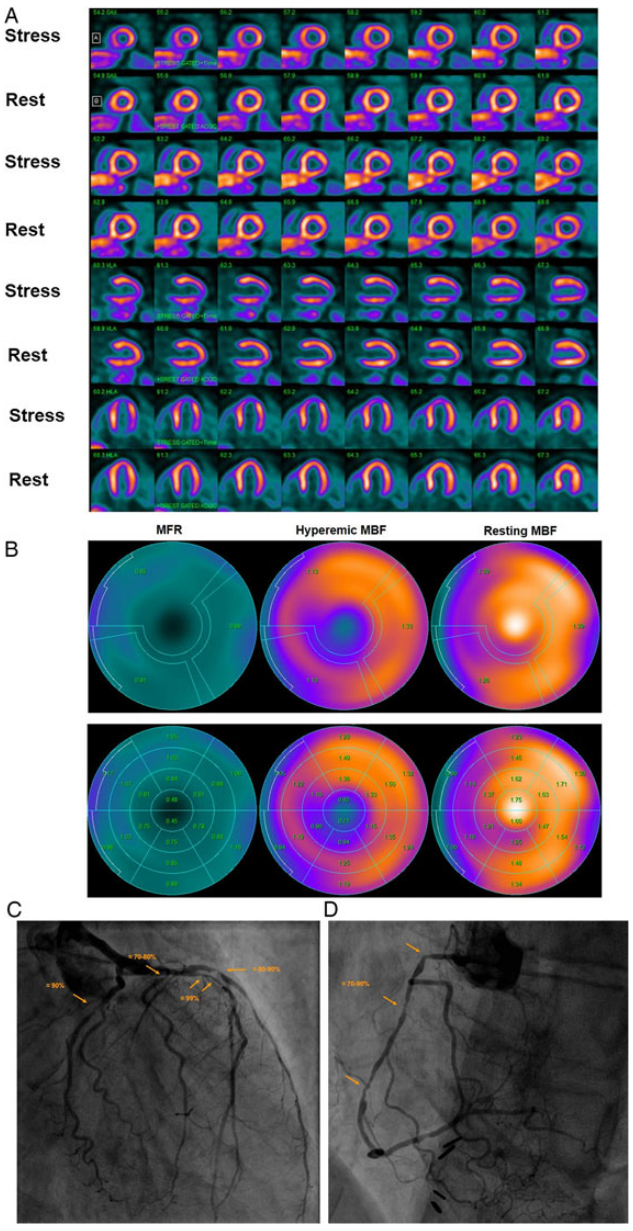

Figure 2 Abnormal stress-rest myocardial perfusion and MBF study with ^{13}N-ammonia PET/CT in a 58-year-old man with typical, effort-induced chest pain. (*A*) Regadenoson-stress and rest ^{13}N-ammonia PET/CT images in corresponding short-axis (top), vertical long-axis (middle), and horizontal long-axis (bottom) slices. On stress images, a moderate-to-severe decrease in myocardial perfusion, involving the antero-septo-apical and apical wall, is realized that becomes reversible on rest images and thus signifies ischaemia in the LAD distribution. (*B*) Regional MBF quantification demonstrates abnormally reduced hyperaemic MBFs and MFR in all three major coronary artery territories of the LAD, LCx, and RCA, respectively (upper panel). Segment MBF analysis unravels a decrease in MBF from the mid- to distal segments with a mean longitudinal MBF gradient during hyperaemic flow in the LAD (0.12 mL/g/min), LCx (0.19 mL/G/min), and RCA (0.30 mL/g/min) (lower-middle panel). (*C*) Invasive coronary angiography of the left coronary artery in this patient demonstrated a long 99% stenosis in the mid-LAD that accounted for the observed stress-induced perfusion defect antero-apical and apical on ^{13}N-ammonia PET/CT perfusion images. In addition, large calibre diagonal branches of the LAD present a ≈70–80% and ≈80–90% stenosis, respectively. The proximal LCx has a proximal ≈80–90% stenosis. Invasively measured FFR of the proximal LCx lesion was abnormally reduced with 0.68 signifying also downstream flow-limiting effects of this lesion. (*D*) Invasive coronary angiography of the right coronary artery demonstrates serial epicardial lesion from the proximal to mid-segments of ≈70–90%, respectively.

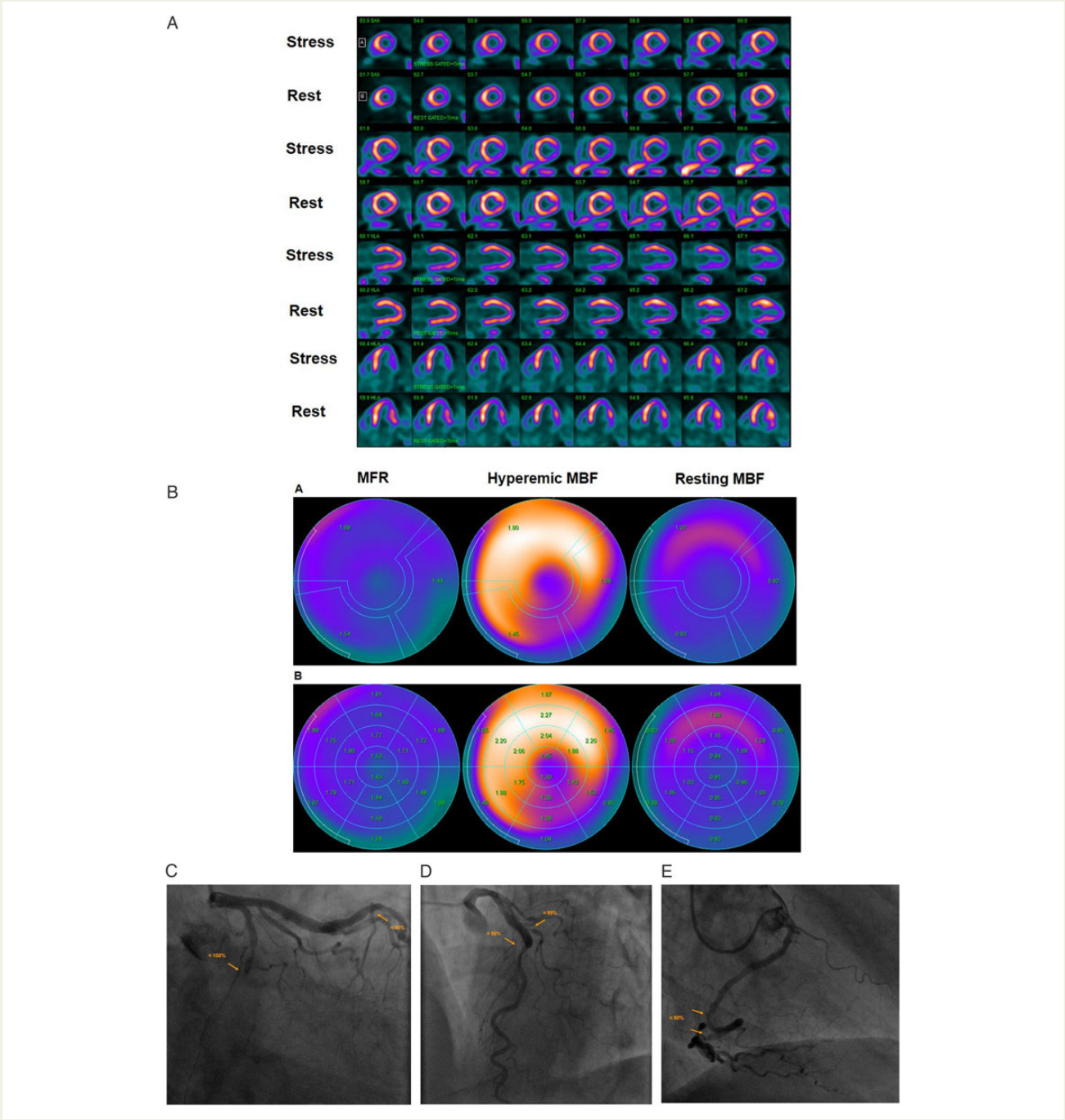

Figure 3 Abnormal stress-rest myocardial perfusion and MBF study with ^{13}N-ammonia PET/CT in a 64-year-old man with atypical chest pain and previous percutaneous intervention of a LAD lesions. (*A*) Regadenoson-stress and rest ^{13}N-ammonia PET/CT images in corresponding short-axis (top), vertical long-axis (middle), and horizontal long-axis (bottom) slices. On rest images, there is a mild decrease of myocardial perfusion of the inferior and inferolateral wall to suggest mild necrosis that, however, markedly worsens during vasomotor stress signifying large size and severe ischaemia in the LCx distribution. (*B*) Regional MBF quantification demonstrates abnormally reduced hyperaemic MBFs and MFR in all three major coronary artery territories of the LAD, LCx, and RCA, respectively (upper panel). Segment MBF analysis outlines a decrease in MBF from the mid- to distal segments with a mean longitudinal MBF gradient during hyperaemic flow in the LAD (0.18 mL/g/min), LCx (0.56 mL/G/min), and RCA (0.09 mL/g/min) (lower-middle panel). (*C*) Invasive coronary angiography of the left coronary artery in this patient demonstrated a complete occlusion of the mid LCx, which is responsible for the stress-induced ischaemia in the inferior and inferolateral wall, and a ≈50% stenosis in the mid-LAD just after a patent stent (left panel). (*D*) An additional left-anterior-oblique projection, however, unmasks a ≈95% stenosis of the proximal diagonal branch in addition to the described LAD lesion (right panel). Invasively measured FFR of the LAD lesions proved to be normal with 0.84. (*E*) Invasive coronary angiography of the right coronary artery demonstrates two serial lesions of ≈50% in the mid- and distal RCA, respectively.

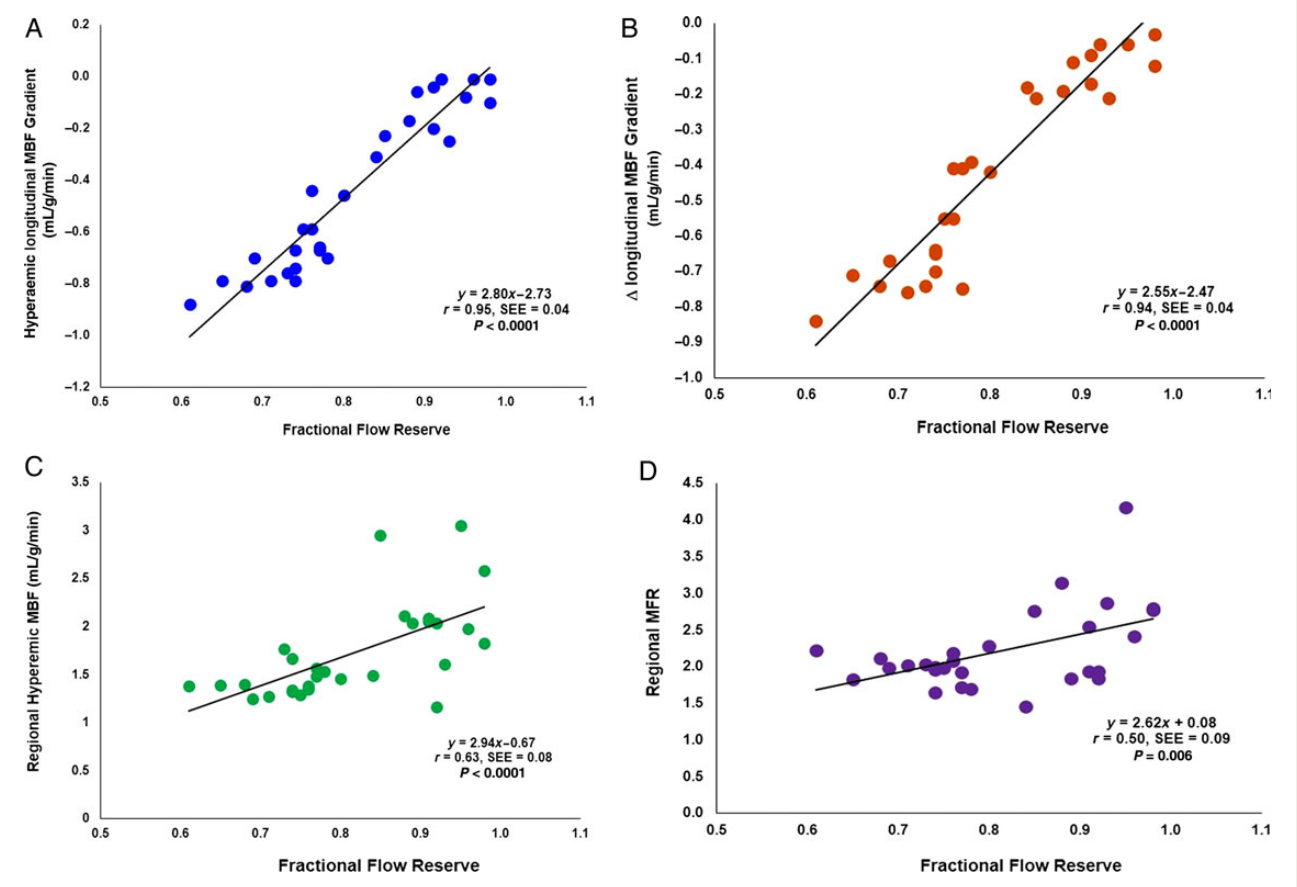

Figure 4 Relationship among hyperaemic longitudinal MBF gradient, Δlongitudinal MBF gradient, hyperaemic MBF, MFR, and severity of invasively determined FFR. Correlation between hyperaemic longitudinal MBF gradient (*A*) and Δlongitudinal MBF gradient (*B*) with corresponding FFR, respectively (negative values on the *y*-axis indicate an increase in longitudinal MBF gradient). In addition, *C* and *D* display the correlation between hyperaemic MBF and MFR with the FFR, respectively. SEE, standard error of the estimate.

gradient during hyperaemic flows was much less pronounced than in regions subtended to less severe epicardial narrowing. As intracoronary resistance relates inversely not only to the vessel diameter according to the Hagen–Poiseuille law but also to the velocity of the blood flow,[15,31] advanced epicardial narrowing is likely to have offset the post-stenotic longitudinal MBF gradient owing to a decrease in hyperaemic flows as described more recently.[1] Such observations outline an uncoupling of the longitudinal MBF gradient from hyperaemic MBFs when an advanced and high-grade stenosis was present. The observed decrease in post-stenotic hyperaemic flow, accompanied by a relative decrease in intracoronary resistance, therefore manifested in a less marked flow gradient than in regions subtended to less severe epicardial lesions in multivessel disease. Notably, in myocardial regions subtended to epicardial vessels without obstructive CAD, the hyperaemic longitudinal MBF gradient was lowest and surprisingly similar to the one in regions with high-grade CAD lesions causing regional perfusion defects. This differs in part from previous investigations with a more pronounced hyperaemic flow gradient in regions with and without diffuse CAD in individuals with subclinical CAD.[22] The exact reason for this discordant observation remains uncertain but is likely to be related to a more severe alterations of microvascular dysfunction in these patients with clinically manifest and severe multivessel CAD than in previous investigations with subclinical CAD.[22] More severe microvascular dysfunction in this study population with advanced and multivessel CAD, associated with markedly reduced hyperaemic MBFs, can be assumed to have offset the magnitude of the hyperaemic longitudinal MBF gradient, resulting in a less marked flow gradient than someone might have expected. Conversely, it is equally possible, at least in part, that the CAD population studied was not large enough or, conversely, that the range of hyperaemic longitudinal MBF gradient between regions with high-grade CAD lesions causing regional perfusion defects and regions without obstructive CAD was not wide enough to result in a statistically significant difference.

Interestingly, in an ^{82}Rubidium PET flow study in patients with subclinical CAD,[32] a regional decrease of myocardial perfusion from the base to the apex of the left ventricle was actually observed at rest but not during dipyridamole-stimulated hyperaemic flows. The reported mild longitudinal decrease in resting myocardial perfusion was related to direct downstream effects of diffuse CAD, which appeared to be overcome during hyperaemic flow stimulation. These observations may be supported by invasive

investigations[33,34] that have described reductions in baseline coronary vasomotor tone in the presence of structural CAD. Differences in structural and/or functional alterations of the coronary circulation, therefore, can indeed be considered as source of a relative and mild fall of regional resting perfusion or flow in a subset of individuals with subclinical CAD.[32] In the current study in patients with clinically manifest and multivessel CAD, a discrete longitudinal MBF gradient was also observed at resting condition that, however, did not differ significantly among myocardial regions. It is intriguing to speculate that in the presence of multivessel CAD, structural alterations of the coronary arteries may have affected downstream coronary flows to a similar extent and/or a compensatory vasodilator adaption of the coronary arteriolar vessels may have set off a more pronounced longitudinal MBF gradient at rest that remains to be further investigated.

Limitations

There are important limitations worthy of considerations in interpreting these clinical observations. First, in view of the relatively small sample size of a selected study population with severe and multivessel CAD, current observations of a close association between invasively determined FFR and PET-determined longitudinal MBF gradient may be seen as a 'proof of principle' study that is likely to stimulate further clinical investigations in this emerging research field. Second, heart rate and blood pressure at rest and during pharmacologically induced hyperaemic flow increases were comparable at the time of the two study sessions, suggesting comparable haemodynamic conditions during invasive FFR and during the PET measurements. Thus, although different pharmacologic agents for hyperaemic flow stimulation were used, such as adenosine for invasive FFR measurements and regadenoson for MBF assessment with PET, differences in haemodynamics can be widely ruled out as potential source of error in this comparison. Third, MBFs in the mid- and mid-distal LV segments were assessed and, thus, the longitudinal MBF gradient was measured over a relatively short longitudinal distance striving to avoid confounding count variability in the basal segments and partial-volume effects in the apical segment on MBF measurements,[1,22] potentially resulting in some underestimation of the longitudinal MBF gradient during pharmacologically-stimulated hyperaemic flows. A more sophisticated and different analysis approach as reported by Gould *et al.*[14] would have been desirable for a more accurate quantification of the extent and severity of the longitudinal flow gradient, needing further investigations. Fourth, novel and recent developments of 3D mapping of MBF, as determined with ^{15}O-water and PET,[35] is less apt or widely without partial-volume effects and flow values can be displayed on a voxel basis. Although this development is likely to afford a more accurate measurement of a longitudinal MBF gradient, it still remains to be tested clinically. Finally, we did not co-acquire coronary CT angiography that would have afforded a more accurate assignment of the coronary vessel segments of the coronary tree to the corresponding myocardial region and MBFs.[36,37] Further, combining 3D fusion of CT-determined coronary morphology and voxel-based MBF would further enable the assessment of a longitudinal flow gradient not only in the post-stenotic myocardial region as in the current study, but also before and after a given CAD lesion. Such a 3D diagnostic approach of fusioned CT-determined coronary morphology and voxel-based MBF could indeed reflect a further step towards the development of a non-invasive FFR.[35,38]

Conclusions

The observed close correlation between a longitudinal MBF gradient during hyperaemic flows and invasively measured FFR supports the validity and value of the longitudinal flow gradient as a non-invasive index of flow-limiting CAD of intermediate severity in multivessel disease needing further clinical investigations.

Acknowledgements

The authors thank Corina Voicu and Jeannie Peters for assisting in the PET studies, and the cyclotron staff for ^{13}N-ammonia production.

Conflict of interest: None declared.

Funding

Departmental fund from Johns Hopkins University (No. 175470), Baltimore, MD, USA.

References

1. Valenta I, Quercioli A, Schindler TH. Diagnostic value of PET-measured longitudinal flow gradient for the identification of coronary artery disease. *JACC Cardiovasc Imaging* 2014;**7**:387–96.
2. Schindler TH. Positron-emitting myocardial blood flow tracers and clinical potential. *Prog Cardiovasc Dis* 2015;**57**:588–606.
3. Schindler TH, Schelbert HR, Quercioli A, Dilsizian V. Cardiac PET imaging for the detection and monitoring of coronary artery disease and microvascular health. *JACC Cardiovasc Imaging* 2010;**3**:623–40.
4. Schindler TH, Dilsizian V. PET-determined hyperemic myocardial blood flow: further progress to clinical application. *J Am Coll Cardiol* 2014;**64**:1476–8.
5. Bengel FM. Leaving relativity behind: quantitative clinical perfusion imaging. *J Am Coll Cardiol* 2011;**58**:749–51.
6. Ziadi MC, Dekemp RA, Williams KA, Guo A, Chow BJ, Renaud JM *et al.* Impaired myocardial flow reserve on rubidium-82 positron emission tomography imaging predicts adverse outcomes in patients assessed for myocardial ischemia. *J Am Coll Cardiol* 2011;**58**:740–8.
7. Fiechter M, Ghadri JR, Gebhard C, Fuchs TA, Pazhenkottil AP, Nkoulou RN *et al.* Diagnostic value of ^{13}N-ammonia myocardial perfusion PET: added value of myocardial flow reserve. *J Nucl Med* 2012;**53**:1230–4.
8. Murthy VL, Naya M, Foster CR, Gaber M, Klein J, Dorbala S *et al.* Association between coronary vascular dysfunction and cardiac mortality in patients with and without diabetes mellitus. *Circulation* 2012;**126**:1858–68.
9. Murthy VL, Naya M, Foster CR, Hainer J, Gaber M, Di Carli G *et al.* Improved cardiac risk assessment with noninvasive measures of coronary flow reserve. *Circulation* 2011;**124**:2215–24.
10. Murthy VL, Naya M, Foster CR, Hainer J, Gaber M, Dorbala S *et al.* Coronary vascular dysfunction and prognosis in patients with chronic kidney disease. *JACC Cardiovasc Imaging* 2012;**5**:1025–34.
11. Schindler TH, Nitzsche EU, Schelbert HR, Olschweski M, Sayre J, Mix M *et al.* Positron emission tomography-measured abnormal responses of myocardial blood flow to sympathetic stimulation are associated with the risk of developing cardiovascular events. *J Am Coll Cardiol* 2005;**45**:1505–12.
12. Gould KL, Johnson NP, Bateman TM, Beanlands RS, Bengel FM, Bober R *et al.* Anatomic versus physiologic assessment of coronary artery disease. Role of coronary flow reserve, fractional flow reserve, and positron emission tomography imaging in revascularization decision-making. *J Am Coll Cardiol* 2013;**62**:1639–53.
13. van de Hoef TP, Siebes M, Spaan JA, Piek JJ. Fundamentals in clinical coronary physiology: why coronary flow is more important than coronary pressure. *Eur Heart J* 2015;**36**:3312–9.
14. Gould KL, Nakagawa Y, Nakagawa K, Sdringola S, Hess MJ, Haynie M *et al.* Frequency and clinical implications of fluid dynamically significant diffuse coronary artery disease manifest as graded, longitudinal, base-to-apex myocardial perfusion abnormalities by noninvasive positron emission tomography. *Circulation* 2000;**101**:1931–9.

15. De Bruyne B, Hersbach F, Pijls NH, Bartunek J, Bech JW, Heyndrickx GR *et al.* Abnormal epicardial coronary resistance in patients with diffuse atherosclerosis but "normal" coronary angiography. *Circulation* 2001;**104**:2401–6.
16. Schindler TH, Facta AD, Prior JO, Prior JO, Campisi R, Inubushi M *et al.* PET-measured heterogeneity in longitudinal myocardial blood flow in response to sympathetic and pharmacologic stress as a non-invasive probe of epicardial vasomotor dysfunction. *Eur J Nucl Med Mol Imaging* 2006;**33**:1140–9.
17. Schindler TH, Facta AD, Prior JO, Cadenas J, Zhang XL, Li Y *et al.* Structural alterations of the coronary arterial wall are associated with myocardial flow heterogeneity in type 2 diabetes mellitus. *Eur J Nucl Med Mol Imaging* 2009;**36**:219–29.
18. Schindler TH, Zhang XL, Vincenti G, Nkoulou RN, Just H, Ratib O *et al.* Diagnostic value of PET-measured heterogeneity in myocardial blood flows during cold pressor testing for the identification of coronary vasomotor dysfunction. *J Nucl Cardiol* 2007;**14**:688–97.
19. Kern MJ. Coronary physiology revisited: practical insights from the cardiac catheterization laboratory. *Circulation* 2000;**101**:1344–51.
20. Scanlon PJ, Faxon DP, Audet AM, Carabello B, Dehmer GJ, Eagle KA *et al.* ACC/AHA guidelines for coronary angiography. A report of the American College of Cardiology/American Heart Association Task Force on practice guidelines (Committee on Coronary Angiography). Developed in collaboration with the Society for Cardiac Angiography and Interventions. *J Am Coll Cardiol* 1999;**33**:1756–824.
21. Danad I, Uusitalo V, Kero T, Saraste A, Raijmakers PG, Lammertsma AA *et al.* Quantitative assessment of myocardial perfusion in the detection of significant coronary artery disease: cutoff values and diagnostic accuracy of quantitative [(15)O]H_2O PET imaging. *J Am Coll Cardiol* 2014;**64**:1464–75.
22. Valenta I, Quercioli A, Vincenti G, Nkoulou R, Dewarrat S, Rager O *et al.* Structural epicardial disease and microvascular function are determinants of an abnormal longitudinal myocardial blood flow difference in cardiovascular risk individuals as determined with PET/CT. *J Nucl Cardiol* 2010;**17**:1023–33.
23. Slomka PJ, Alexanderson E, Jacome R, Jiménez M, Romero E, Meave A *et al.* Comparison of clinical tools for measurements of regional stress and rest myocardial blood flow assessed with ^{13}N-ammonia PET/CT. *J Nucl Med* 2012;**53**:171–81.
24. Germano G, Kiat H, Kavanagh PB, Moriel M, Mazzanti M, Su HT *et al.* Automatic quantification of ejection fraction from gated myocardial perfusion SPECT. *J Nucl Med* 1995;**36**:2138–47.
25. Choi Y, Huang SC, Hawkins RA, Kuhle WG, Dahlbom M, Hoh CK *et al.* A simplified method for quantification of myocardial blood flow using nitrogen-13-ammonia and dynamic PET. *J Nucl Med* 1993;**34**:488–97.
26. Martinez-Moller A, Zikic D, Botnar RM, Bundschuh RA, How W, Ziegler SI *et al.* Dual cardiac-respiratory gated PET: implementation and results from a feasibility study. *Eur J Nucl Med Mol Imaging* 2007;**34**:1447–54.
27. Schindler TH. Myocardial blood flow: putting it into clinical perspective. *J Nucl Cardiol* 2015 Dec 28 [Epub ahead of print].
28. Hernandez-Pampaloni M, Keng FY, Kudo T, Sayre JS, Schelbert HR. Abnormal longitudinal, base-to-apex myocardial perfusion gradient by quantitative blood flow measurements in patients with coronary risk factors. *Circulation* 2001;**104**:527–32.
29. Gould KL, Lipscomb K. Effects of coronary stenoses on coronary flow reserve and resistance. *Am J Cardiol* 1974;**34**:48–55.
30. Gould KL, Lipscomb K, Hamilton GW. Physiologic basis for assessing critical coronary stenosis. Instantaneous flow response and regional distribution during coronary hyperemia as measures of coronary flow reserve. *Am J Cardiol* 1974;**33**:87–94.
31. Johnson NP, Kirkeeide RL, Gould KL. Is discordance of coronary flow reserve and fractional flow reserve due to methodology or clinically relevant coronary pathophysiology? *JACC Cardiovasc Imaging* 2012;**5**:193–202.
32. Johnson NP, Gould KL. Clinical evaluation of a new concept: resting myocardial perfusion heterogeneity quantified by Markovian analysis of PET identifies coronary microvascular dysfunction and early atherosclerosis in 1,034 subjects. *J Nucl Med* 2005;**46**:1427–37.
33. Schachinger V, Zeiher AM. Quantitative assessment of coronary vasoreactivity in humans in vivo. Importance of baseline vasomotor tone in atherosclerosis. *Circulation* 1995;**92**:2087–94.
34. Tousoulis D, Davies GJ, Tentolouris C, Crake T, Lefroy DC, Toutouzas P. Effects of inhibition of nitric oxide synthesis in patients with coronary artery disease and stable angina. *Eur Heart J* 1997;**18**:608–13.
35. Kajander SA, Joutsiniemi E, Saraste M, Pietila M, Ukkonen H, Saraste A *et al.* Clinical value of absolute quantification of myocardial perfusion with (15)O-water in coronary artery disease. *Circ Cardiovasc Imaging* 2011;**4**:678–84.
36. Nakazato R, Otake H, Konishi A, Iwasaki M, Koo BK, Fukuya H *et al.* Atherosclerotic plaque characterization by CT angiography for identification of high-risk coronary artery lesions: a comparison to optical coherence tomography. *Eur Heart J Cardiovasc Imaging* 2015;**16**:373–9.
37. Cheezum MK, Ghoshhajra B, Bittencourt MS, Hulten EA, Bhatt A, Mousavi N *et al.* Anomalous origin of the coronary artery arising from the opposite sinus: prevalence and outcomes in patients undergoing coronary CTA. *Eur Heart J Cardiovasc Imaging* 2017;**18**:224–35.
38. Danad I, Raijmakers PG, Harms HJ, van Royen N, Lubberink M, Boellaard R *et al.* Impact of anatomical and functional severity of coronary atherosclerotic plaques on the transmural perfusion gradient: a [^{15}O]H_2O PET study. *Eur Heart J* 2014;**35**:2094–105.